Conf-9110242--1

ANL/BC--72031

DE92 001980

Received by OSTI

OCT 2 8 1991

X-RAY REFLECTIVITY STUDIES OF THE METAL/SOLUTION INTERPHASE*

H. You, Z. Nagy, C. A. Melendres, D. J. Zurawski,
R. P. Chiarello, R. M. Yonco, H. K. Kim,** and V. A. Maroni

Argonne National Laboratory
Divisions of Materials Science and Chemical Technology
Argonne, Illinois 60439-4837

September, 1991

To be submitted to the Electrochemical Society Symposium Proceedings Volume
"X-Ray Methods in Corrosion and Interfacial Electrochemistry"

DISCLAIMER

This report was prepared as an account of work sponsored by an agency of the United States Government. Neither the United States Government nor any agency thereof, nor any of their employees, makes any warranty, express or implied, or assumes any legal liability or responsibility for the accuracy, completeness, or usefulness of any information, apparatus, product, or process disclosed, or represents that its use would not infringe privately owned rights. Reference herein to any specific commercial product, process, or service by trade name, trademark, manufacturer, or otherwise does not necessarily constitute or imply its endorsement, recommendation, or favoring by the United States Government or any agency thereof. The views and opinions of authors expressed herein do not necessarily state or reflect those of the United States Government or any agency thereof.

*Work sponsored the Division of Materials Sciences, Office of Basic Energy Sciences, U. S. Department of Energy, under Contract W-31-109-Eng-38.

**Permanent address: Department of Physics, Pusan National University, Pusan, Korea.

MASTER

DISTRIBUTION OF THIS DOCUMENT IS UNLIMITED

X–RAY REFLECTIVITY STUDIES OF THE METAL/SOLUTION INTERPHASE

H. You, Z. Nagy, C. A. Melendres, D. J. Zurawski,
R. P. Chiarello, R. M. Yonco, H. K. Kim,* and V. A. Maroni
Argonne National Laboratory
Divisions of Materials Science and Chemical Technology
Argonne, Illinois 60439–4837

We have designed an electrochemical cell that permits x–ray scattering studies in a transmission geometry under *in–situ* electrochemical control and have performed x–ray specular reflectivity studies of several metal/solution interphases as a function of electrochemical potential. For the copper/solution interphase, we found that the reflectivity changes upon oxidation and reduction, indicating a phase transition between copper and copper oxide at the interphase. We also found that the thickness of the pure copper and the roughness of the interfaces exhibited electrochemical irreversibility that is consistent with the potentials for the oxidation waves in the anodic sweep and the reduction waves in the cathodic sweep of the voltammogram. A standard Fresnel expression for the x–ray specular reflectivity was applied in the data analysis, and a smoothly varying Lorentzian interface profile was used for the individual rough interfaces. Furthermore, an incoherent average was used to include the effect of *correlated roughness* between a pair of interfaces. Preliminary results are also presented for the silver/solution and platinum/solution interphases.

The substantial increase in x–ray intensity available at synchrotron sources compared to conventional rotating anode sources has created many new applications for x–ray techniques, such as x–ray scattering, absorption spectroscopy, standing waves, and others. Because x–rays can penetrate a macroscopic distance through aqueous media, the application of these techniques to electrochemically controlled metal/solution interphases has become popular. Some recent examples can be found in the literature for x–ray absorption (1), x–ray standing wave (2), and x–ray scattering techniques (3,4), and in recent reviews (5–8). In particular, the use of x–ray scattering techniques to study electrochemical interphases allows one to obtain structural and morphological information at the microscopic level.

*Permanent address: Department of Physics, Pusan National University, Pusan, Korea.

In most prior x-ray scattering studies (3,4), the electrochemical cells were designed to perform the measurements in the reflective geometry shown schematically in Fig. 1a. The window of the cell through which x-rays pass is parallel to the interface of interest. It is analogous to Bragg geometry (9) for the single crystal scattering case where the interface of interest is considered as a Bragg plane. However, it is also possible to perform the x-ray scattering studies in a transmission geometry (Laue geometry) where the incoming x-rays pass through a window perpendicular to the interface of interest and the outgoing x-rays pass through a second perpendicular window. The cell geometry for the Laue case is shown schematically in Fig. 1b. The transmission geometry can complement or improve upon the reflective geometry in suitability for *in-situ* potential control as well as in accessibility to small scattering angles.

The reflection geometry has several disadvantages from the standpoint of desirable electrochemical practice. The current distribution over the working electrode surface is very nonuniform because of the geometrical arrangement of the electrodes and the large ohmic resistance in the electrolyte gap. It is common practice with this type of cell, to expand the electrolyte gap by inflating the membrane (or withdrawing the electrode assembly) during electrochemical manipulations. However, during the measurements with x-rays, the electrolyte gap is constricted to a small fraction of a mm, which could lead to the loss of meaningful potential control. A cell designed for transmission geometry (Fig. 1b) alleviates these problems at the price of increased attenuation of the beam intensity, and that can be minimized by choosing an optimum cell thickness.

The transmission geometry is also advantageous from the x-ray scattering standpoint. (i) In the transmission geometry (Fig. 1b), x-rays reflect to the detector from the electrochemical interface only, while in the reflection geometry (Fig. 1a), x-rays reflect from the air/membrane and membrane/solution interfaces as well as the interface of interest. Therefore, the reflectivity data in transmission geometry can be interpreted directly, while the data obtained in reflection geometry require deconvolution or subtraction of the interference from air/membrane and membrane/solution interfaces. Furthermore, the nature of those additional interfaces may also vary as the experimental conditions change, which can compromise the correct interpretation of the data. (ii) Reflectivities measured in transmission geometry require little absorption correction because the path length of x-rays is nearly constant over the angular range of interest, while with the reflection geometry the path length changes sharply for small angles. (iii) Since the attenuation is an exponential function of path length, there is a tendency for the diffuse background to rise rapidly at small scattering angles in the reflection geometry; therefore, the total signal gets reduced by absorption but the diffuse background from the top membrane and the membrane/solution interface is hardly attenuated, resulting in a low signal-to-background ratio at small angles. In the transmission geometry, the diffuse background is attenuated as much

as the signal, and the signal–to–background ratio remains constant over the full angular range of interest. The low signal–to–background ratio is particularly important for in–plane scattering studies at glancing angles when the expected signal is very weak.

One apparent advantage of the reflection geometry is that there is no severe restriction on the size of the sample surface, while in the transmission case, the width of the cell must be optimized to the order of the absorption length of x–rays, which is a few mm for readily available x–ray energies. Our cell thickness was chosen to be equal to an absorption length of 1 Å x–rays. However, sample size is hardly an advantage because the small spot size of a focused synchrotron beam. The main advantage of the reflection geometry is accessibility to high scattering angles.

EXPERIMENTAL

We have designed an electrochemical cell for ***in–situ*** x–ray reflectivity measurements using the transmission geometry, as shown in Fig. 2. The cell is a layer–type, sandwich configuration, consisting of a Teflon center section that houses the electrodes and shapes the electrolyte cavity, surrounded on both sides by thin plastic membranes; the membranes are pressed in place by a pair of Teflon inner frames, which, in turn, are supported by a pair of outer metal frames. The schematic view in Fig. 2 shows only the center section and one of the two sets of framing pieces of the cell. The pair of inner and outer frames are cut with appropriately shaped slits to permit the x–rays to enter and exit the cell through the membrane cell windows in a range of 45°. The assembly is held together by bolts that compress the inner frames and the center section to provide a solution–tight seal around the edges. The outer frames are also equipped with appropriate mounting fixtures to attach the cell to a four–circle x–ray spectrometer.

The electrolyte cavity is so shaped as to accommodate rotation of the cell by 90° in either direction and still provide gas space above the electrolyte with the working and counter electrodes fully submerged. For the same reason, there are two vent holes, one in each upper corner of the electrolyte cavity. The cell is further equipped with solution–fill and gas–bubbler tubes, and connections to purge or fill the space below the working electrode. These input/output connections are made of Teflon tubing that is tightly fitted into holes drilled in the Teflon center section, their functions are generally interchangeable. Electrical contact is made at both ends of the working electrode using lead wires that are pressed against the bottom of the electrode. The inert metal wire counter electrode is positioned above the working electrode surface traversing its full length to provide a uniform current distribution. The lead wires are sealed in a Teflon sheath that forms a tightly fitting, sliding seal in the center section. The reference electrode is positioned close to the working electrode surface to ensure a small uncompensated ir–drop in the solution. Either internal or external reference electrodes can be used. Internal reference can be, for

example, chloride or oxide coated silver wire sheathed in Teflon tubing except for a few mm at the working end. In the case of an external reference electrode, a small Teflon tube can serve as both Luggin tip and solution bridge.

The cell design shown in Fig. 2 illustrates the use of a single crystal working electrode ($\sim 3 \times 3 \times 10$ mm). We also used thin film electrodes. Several commercially available polished substrate materials, such as single crystal sapphire, borosilicate glass, fused silica, single crystal silicon, and unpolished float glass (all $\sim 3 \times 2 \times 36$ mm in dimension) were used as the substrates. The x-ray reflectivity of each type of substrate was measured with a rotating anode source to determine the roughness of the substrate. We found that the sapphire, fused silica, and borosilicate substrates were acceptable ($\sim$10 Å rms), but silicon, at less than 3 Å rms, was clearly the best in terms of smoothness. The substrates were cleaned repeatedly with alcohol, acetone, and water in an ultrasonic cleaner. Metal films were applied to the substrate by standard vapor deposition techniques. Then the samples were stored individually in sealed glass capsules filled with inert gas to protect them from oxidation prior to mounting in the cell. The cell center section suitable for film electrodes and other details of the cell design are given elsewhere (10).

Several polymer films were tested for their suitability as membrane materials. Two major requirements of these materials are (i) durability under prolonged exposure to the intense x-ray beam produced by the synchrotron, and (ii) chemical inertness to the concentrated acid cleaning solutions and to the test electrolyte. Eight membrane materials were tested by exposure to a focused 12 keV x-ray beam, for various lengths of time. The approximate photon flux was 7×10^{14} photons/mm^2/h. Following exposure, the films were examined under an optical microscope for extent and type of damage. The results of the test are given in Table I.

The results indicate that only Kapton and Mylar are not damaged by the x-rays over the required time scale, while Tefzel shows only minor damage after prolonged exposure. However, considering the criteria of chemical inertness, Kapton FN was judged to be the most satisfactory membrane material. Kapton FN, a Teflon coated Kapton membrane, combines the radiation resistance of Kapton with the chemical inertness of Teflon. This permits cleaning the cell with strong acids prior to the experiment. During a long x-ray exposure, the Teflon coating perforates, but this exposes only a small area of the Kapton to the relatively mild test solution. Two membrane materials were used in our experiments. Teflon FEP was used with metal film electrodes, and Kapton FN was used with the single crystal electrode. Teflon membranes were found to puncture after about 24 hours of use, while Kapton was used without puncture for several days.

All x-ray experiments were carried out using the National Synchrotron Light Source at Brookhaven National Laboratory. The film electrode studies were carried out at the X22C beamline and the single-crystal studies at the X10B beamline.

THEORETICAL

A detailed discussion of the theoretical background for these measurements and the derivation of the reflectivity equations used for the evaluation of the experimental data are given elsewhere (11); only a very brief description of the theory is given here. Although the dynamic solution of the x-ray reflectivity from a series of interfaces is possible, the single scattering (kinematic) limit has been widely used due to its simplicity. Since there is no double scattering contribution and the reflection coefficient from an individual interface drops rapidly, the single scattering limit is a good approximation even quite close to the critical angle. (In this work we found that the kinematic approach gave good results starting at ~0.03 Å^{-1} above the critical angle.) Also, the kinematic approach clearly identifies some of the important physics in the equation, which makes it more understandable than the dynamic solution. We treat only the scattering angles that are larger than the critical angle of the highest density material in the layers and work with sufficiently thin total layers that we can neglect absorption.

The scattered x-ray intensity from a total of N interfaces in terms of scattering amplitude (V_n) and phase (ϕ_n) from the interface between the nth and (n+1)th media is considered in terms of the momentum transfer (known as the refractive correction) inside the nth medium as $Q_n = \sqrt{Q^2 - Q_{cn}^2}$, where $Q_{cn} = 0.0289\sqrt{Z_E A \rho_n}$ from Snell's law for small reflection angles. Z_E is the total number of electrons whose binding energy is smaller than the x-ray energy used for the measurements, and A and ρ are the atomic weight and density of the medium, respectively.

In reality, the surface is rough compared to the x-ray wavelength (see Fig. 3b) and the roughness modifies the reflectivity. Since many evaporated films grow predominantly in crystallographic planes parallel to the substrate, the flat area in Fig. 3b can be imagined as the growth plane. Then the amplitudes of the x-rays reflected from each flat area must be added within the x-ray coherence length. The reflected amplitude from each growth plane will have a phase advance or delay depending on its position. By assuming that there is a definite average interface position we can take an average of the amplitude with $\mathcal{P}(z)$, the probability distribution function for the flat surface, and $P(Q)$, its Fourier transform. The most commonly used distribution is the Gaussian. However, a Gaussian distribution is not unique, and we have shown that a Lorentzian distribution gives better results for the evaporated thin films used in our measurements (11).

The x-ray coherence length can vary from several hundred to tens of thousands of angstroms depending on the instrumental resolution (Longitudinal coherence length for our experimental set up was about 5000 Å). However, this length scale is significantly smaller than the size of the sample, and it is often necessary to consider an incoherent average over many independent x-ray photons. Of course, if the sample is homogeneous enough so that there is no distinction from one part

of the sample to another, then this averaging is unnecessary. In many cases, however, the samples are sufficiently inhomogeneous over their macroscopic dimensions so that incoherent averaging is necessary. (For the case of vapor deposited films, variations in the thickness can occur due to inhomogeneous evaporation.) In this case, the phase angle needs averaging following the arguments given above. Thus, the reflectivity finally becomes

$$I = \sum_{n=1}^{N} V_n^2 P_n^2(Q_n) + 2 \sum_{m<n}^{N} V_m V_n P_n(Q_n) P_m(Q_m) P_{m,n}(Q) \cos \left\{ \sum_{j=n+1}^{m} Q_j(\bar{z}_j - \bar{z}_{j-1}) \right\}$$

Where, $P_{m,n}$ is the interface/interface correlation function over the large length scale, and $\bar{z}_j$ is an effective thickness of medium j. For independently rough interfaces the incoherent average will increase the effective interface width, and the oscillations will damp out more rapidly at higher momentum transfer. However, a pair of interfaces whose roughnesses are strongly correlated (known as conformally rough interfaces) will not damp out as rapidly. An example of an ideal conformally rough interface is shown in Fig. 3c. We assume that the conformality exists over the entire sample having a much larger length scale than the coherence length of the x-rays. Therefore, conformal roughness can alter the specular reflectivity, and we have included this effect to adequately analyze our data in the event of a possible non-uniform thickness in the evaporated metal films.

RESULTS AND DISCUSSION

We have investigated several metal/solution interphases in various degrees of detail. We used a nickel–chromium sandwich film electrode to demonstrate the feasibility of *in-situ* x-ray reflectivity measurements on multilayered films under an aqueous solution. A silver film electrode was used to demonstrate the sensitivity of the measurements to morphological changes at the electrode surface. A detailed investigation was carried out of the copper oxidation/reduction process. And, finally, preliminary experiments were carried out to observe the roughening of a platinum single crystal surface induced by electrochemical oxidation/reduction.

Chromium-nickel film

We investigated a known system to test the effect of the presence of the solution on x-ray reflectivity and to demonstrate the capability to resolve multilayered interfaces (10,11). The sample was a layered composite of a thick nickel film over a thin chromium film on a polished borosilicate glass substrate. The nickel surface in 0.1 M NaOH solution at an open circuit condition is expected to have only a few monolayers of surface oxide, therefore, the reflectivity should not be affected by the oxide layer over the Q range of this study. Figure 4 shows reflectivity scans of the sample with and without electrolyte present. Reflectivity is plotted as a function of

the momentum transfer, $Q = (4\pi/\lambda)\sin\theta$. The high–frequency interference fringes in Fig. 4 are due to the total film thickness and the low–frequency oscillations are due to the thin chromium under–layer. The top curve is the reflectivity under dry nitrogen, and the bottom one is under aqueous 0.1 M NaOH. Several features are worth noticing in Fig. 4: (i) The intensity drops by a factor of 20 when we introduce the solution. This ratio can be exactly calculated (11) for the 1.48 Å x–ray wavelength used. (ii) There is a small shift in critical angle as expected from the decrease in the contrast of the electron density between air/nickel and solution/nickel. (iii) The solution scan tracks the top scan without any other additional features. (iv) Although it is not evident from the figure, the decrease in the signal to background ratio for the solution scan was less than 10% over the measured Q range. The diffuse scattering from the solution was very small for this Q range and for the resolution used. In addition, the diffuse scattering is attenuated almost as much as the signal because of a similar path length through the solution (10). These observations indicate that the x–ray intensity attenuation due to the solution does not complicate interpretation of the data.

Silver film

Several preliminary experiments were carried out to demonstrate the feasibility of the observation of the electrochemical formation of a passive oxide film (10). The working electrode was a 250 Å silver film deposited on polished silicon(100) single crystal, and the solution was aqueous borate buffer (pH=8.4). The reflectivity spectra are shown in Fig. 5. The first spectrum was taken at −0.8 V on a reduced metal surface, this spectrum was reproduced at 0.0 V, a potential where oxide formation is still absent, and finally the spectrum of the oxidized silver was obtained at 0.5 V. The significant difference in the reflectivity at reducing and oxidizing potentials clearly demonstrates the sensitivity of the measurements to the changes in surface morphology caused by the electrochemical reactions. The smooth interference pattern at the oxidizing potential indicates that the film/solution interface roughens as oxidation occurs at the interphase. Other experiments with silver–film electrodes are described elsewhere (11).

Copper film

Figure 6 shows a voltammogram of the thin-film copper electrode in borate buffer solution (pH=8.4). Anodic dissolution leading to the formation of Cu(I) and Cu(II) surface oxides is indicated by the anodic waves, subsequent reduction of these films occurs during the cathodic scan. At the 10 mV/sec scan rate, the total charge transferred under either peak is approximately 1 coulomb. The anodic scan leads to the formation of two oxidation states of copper at −0.1 and 0 V, respectively, and the subsequent reverse cathodic scan reduces the oxide films at −0.3 and −0.5 V.

Figure 7 shows a series of x–ray reflectivity scans taken at several potentials between −0.8 V to 0.4 V, with a nominally 250 Å vapor–deposited copper film on Si(100) single–crystal support. The solid lines are calculated by a curve–fitting procedure as discussed below, and only one out of every five data points are shown for the sake of clarity.

The top scan was made under open circuit condition (−0.12 V). Subsequently, the potential was changed to −0.8 V at a sweep rate 10 mV/sec. When the current through the electrode reached a steady state value of less than 1 μA, a reflectivity scan was made while holding the potential at −0.8 V. The amplitude of the oscillation in the reflectivity slightly increased indicating that the solution/copper interface is becoming less rough. Then, at the same sweep rate, the potential was changed to 0.4 V and a reflectivity scan was made again when the current reached steady state. At this potential oxide formation is expected, and the reflectivity indeed exhibited a dramatic change from the −0.8 V reflectivity curve. The oscillation frequency became smaller and the oscillation amplitude decreased. Again the potential was changed to −0.8 V, after which the amplitude and frequency of the reflectivity oscillation nearly recovered to the previous reflectivity at −0.8 V.

Subsequently, the potential was changed in a stepwise fashion and reflectivity scans were made at −0.8 V, −0.6 V, −0.4 V, and −0.2 V. There is little change in the reflectivity until the potential reaches −0.2 V. This is consistent with the voltammogram. As the potential reaches to 0 V, the reflectivity drastically changes. Then the reflectivity changes only slightly until the potential reaches 0.4 V. In the cathodic sweep, the reflectivity does not recover its oscillation amplitude until the potential reaches −0.4 V, which is also consistent with the positions of the cathodic waves. At the potential of −0.8 V, the film nearly recovers its original oscillatory behavior.

The reflectivity data in Fig. 7 were analyzed by curve fitting to the reflectivity equation developed for three interfaces, i.e., solution/copper oxide, copper oxide/copper, and copper/silicon (11). As mentioned earlier, all the interfaces considered in our data analysis are assumed to be Lorentzian. A few assumptions have been made in the curve fitting. We assumed that the thickness of the oxide is uniform over macroscopic distances. We further assumed that the total mass of copper is conserved by neglecting the possible small amount of copper oxide that is lost during the electrochemical cycling. The total amount of copper was then constrained to 285 Å, the value obtained from a reflectivity scan with nitrogen gas rather than solution in the cell, prior to the electrochemical experiments. The density of the electrochemically formed oxide film was constrained to 5.5 g/cm^3, the value obtained from the scan at 0.4 V. The density of 5.5 g/cm^3 is reasonable since it is known that the passive film is composed of mainly Cu_2O, mixed with some CuO and $Cu(OH)_2$. The roughness of the silicon/copper interface was assumed to be zero because the roughness of the bare silicon surface was found to be less than 3 Å. The thickness

of the pure copper layer, the roughness of the copper/oxide and oxide/solution interfaces, and the conformal roughness of these two interfaces were than determined from the reflectivity data using a standard curve-fitting procedure.

The resulting parameters for the three-interface treatment of the copper film data are listed in Table II. Since the amount of charge transfer during the voltammogram indicates that no oxide should remain at the reducing potentials, the small amount of residual film (~10 Å) might be indicative of the presence of a porous copper region where some of the oxide film had formerly existed at an oxidizing potential. It also suggests that the kinetics associated with the metal layer redevelopment might be too slow at room temperature for smoothing of the interface to occur.

The results indicate that the roughness of the oxide/solution and copper/oxide interfaces gradually increases as the potential is cycled. This means that the interface on a microscopic scale (within the x-ray coherence length) continuously roughens as the sample undergoes electrochemical oxidation and reduction. However, two parameters, the thickness of the copper and the correlated roughness, show interesting electrochemical irreversibility effects. These two parameters are plotted in Fig. 8. The square symbols are from the top 3 scans in Fig. 7, and the circled symbols are for the rest of the scans. An open symbol indicates that the scan was made during or at the end of the anodic sweep and a filled symbol indicates that the scan was made during, or at the end of, the cathodic sweep.

The thickness of the pure copper decreases upon oxidation (while the thickness of the oxide increases) and increases upon reduction. The copper thickness also shows an electrochemical irreversibility of ~0.3 V as is seen in Fig. 8 by the lines used to guide the eye. This irreversibility is in agreement with the irreversibility exhibited by the anodic and cathodic waves in the voltammogram. The measured thickness of the passive film is 20~30 Å at the highest oxidation potential used in the study. The change in the thickness of the copper directly represents the total charge transfer due to the oxidation. Since the number of atoms in a (111) plane is $\sim 10^{15}$ for our sample size, the integrated charge transfer below the anodic waves, which is ~1 coulomb, corresponds to ~10 layers of (111) planes or ~30 Å.

Figure 8b shows the correlated roughness, and that it increases upon oxidation. A possible explanation for this increased roughness is the following. The film is composed of many copper single crystallites, that are randomly oriented about the surface normal and connected by grain boundaries. The average size of the particles can be hundreds to thousands of angstroms. The fact that the correlated roughness increases upon oxidation suggests that the oxidation occurs at the grain boundaries. Grain boundary oxidation will effectively increase the long length-scale roughness and be reflected in the increased correlated roughness.

The correlated roughness also shows irreversibility, but the irreversibility loop does not close and the correlated roughness remains larger after the complete cycle. This indicates that the grain boundaries only partially recover their original morphology upon reduction. That is, the once roughened grain boundaries do not completely recover the original flatness upon reduction and the interface becomes progressively rougher upon repeated oxidation and reduction. More details of these experiments are given elsewhere (11,12).

Platinum single crystal

Oxidation of the precious metals is one of the most extensively studied subjects in electrochemistry due to its scientific interest. The precious metals, such as platinum, do not form more than a monolayer of oxide in the ambient environment. However, charge transfer measurements have shown that a much thicker layer of oxide can form in a solution. In our preliminary measurements on Pt(111) oxidation in 0.1 M CsF solution, we found that the initially flat surface completely recovers its original surface after reduction of the oxide film formed at potentials up to 500 mV versus Ag/AgCl (3 M KCl) reference electrode; but the surface irreversibly roughens upon a cycle of the potential beyond 500 mV.

A series of crystal–truncation–rod (13) scans is shown in Fig. 9. The scans were made at 0 mV, after oxidation at the potential indicated and reduction at −800 mV. The abscissa unit is the reciprocal lattice unit of platinum in the hcp unit cell (roughly $Å^{-1}$). The scans show no change up to the 500 mV cycle, i.e., the surface remains flat. Then the surface progressively roughens following the cyclic potential control beyond 500 mV, as indicated by the increased drop in reflectivity with L.

Our electrochemical measurements (cyclic voltammetry) of the oxygen coverage of the platinum surface indicated that a full monolayer of oxide coverage is not achieved at a potential negative to ~600 mV, suggesting that oxidation/reduction of less than a monolayer of oxide film will not roughen the originally flat surface, but the surface will roughen if more than a monolayer of oxide is formed/reduced. More detailed measurements on this system will be reported in the future (14).

ACKNOWLEDGMENTS

This work was performed under the auspices of the Division of Materials Sciences, Office of Basic Energy Sciences, U. S. Department of Energy, under Contract No. W-31-109-Eng-38, and was carried out in part at the National Synchrotron Light Source, Brookhaven National Laboratory, which is supported by the U. S. Department of Energy, Division of Materials Sciences and Division of Chemical Sciences. We are grateful to D. M. Gruen and P. A. Montano for their continued support and encouragement.

REFERENCES

1. L. Bosio, R. Cortes, A. Defrain, and M. Froment, *J. Electroanal. Chem. Interfacial Electrochem.,* **180**, 265 (1984).
2. G. M. Bommarito, J. H. White, and H. D. Abruna, *J. Chem. Phys.,* **94**, 8280 (1990).
3. M. F. Toney, J. G. Gordon, M. G. Samant, G. L. Borges, O. R. Melroy, L.-S. Kau, D. G. Wiesler, D. Yee, and L. B. Sorensen, *Phys. Rev.,* **B42**, 5594 (1990) and references therein.
4. B. M. Ocko, J. Wang, A. Davenport, and H. Isaacs, *Phys. Rev. Lett.,* **65**, 1466 (1990).
5. J. Robinson, in "Spectroelectrochemistry, Theory and Practice," R. J. Gale, Editor, p. 9, Plenum Press, New York (1988).
6. H. D. Abruna, in "Modern Aspects of Electrochemistry," J. O'M. Bockris, R. E. White, and B. E. Conway, Editors, No. 20, p. 265, Plenum Press, New York (1989).
7. C. Gutierrez and C. Melendres, Editors, "Spectroscopic and Diffraction Techniques in Interfacial Electrochemistry," Kluwer Academic Publishers, Boston, (1990).
8. H. D. Abruna, Editor, "Electrochemical Interfaces: Modern Techniques for In-Situ Interface Characterization," VCH Publishers, New York, (1991).
9. B. W. Batterman and H. Cole, *Rev. Mod. Phys.,* **36**, 681 (1964).
10. Z. Nagy, H. You, R. M. Yonco, C. A. Melendres, W. Yun, and V. A. Maroni, *Electrochim. Acta,* **36**, 209 (1991).
11. H. You, C. A. Melendres, Z. Nagy, V. A. Maroni, W. Yun, and R. M. Yonco, to be published.
12. C. A. Melendres, H. You, V. A. Maroni, Z. Nagy, and W. Yun, *J. Electroanal. Chem. Interfacial Electrochem.,* **297**, 549 (1991).
13. H. You, in "Proceedings of Second International Conference on Surface X-Ray and Neutron Scattering," H. Zabel and I. K. Robinson, Editors, Bad Honnef, Germany, June 25-28, 1991, Pergamon Press. Submitted for publication.
14. H. You et al., to be published.

Table I.
Membrane Damage Due to X–Ray Exposure

Type[b]	Membrane Thickness (μm)	Rating[a] after exposure for times indicated 9h	18h	50h	106h
Kapton HN	25	0	0	0	0
Mylar EL	25	0	0	0	0
Mylar D	23	0	0	0	0
Tefzel LZ	25	0	0	0	1
Teflon FEP	25	2	1	1	3
Teflon TFE	25	1	0	1	4
Polypropylene	6.3	3	1	5	3
Kapton FN[c]	37.5	1	5	5	4

a) Observations with optical microscope: 0=no visible damage, 1=clouding, 2=clouding, cracks developing, 3=cracks completely penetrate through membrane, 4=puncture with clouding and extensive cracking, 5=clearly visible circular hole.

b) All membranes, except polypropylene, were manufactured by Du Pont.

c) Kapton FN is a sandwich consisting of 12.5 μm of Kapton HN between two sheets of 12.5 μm Teflon FEP. Damages indicated are for the outer Teflon layers only; the Kapton layer was undamaged.

Table II.
Curve–Fitted Results for Copper Oxidation/Reduction

Potential (V)	Roughness (Å) Conformal	Oxide	Copper	Thickness (Å) Copper	Oxide
-0.12	16(2)	4.4(5)	4.6(4)	273(2)	12(2)
-0.80	11(1)	4.6(5)	3.3(5)	285(2)	0(2)
0.40	25(1)	4.4(5)	5.6(6)	250(3)	35(2)
-0.80	12(1)	4.6(5)	5.3(6)	276(2)	9(2)
-0.60	12(1)	4.7(5)	5.7(6)	272(2)	13(2)
-0.40	12(1)	4.4(5)	6.1(5)	272(2)	13(2)
-0.20	13(1)	5.2(5)	6.3(5)	275(2)	10(2)
0.00	30(2)	4.5(5)	5.4(6)	255(7)	30(7)
0.20	24(2)	5.5(5)	9.6(9)	252(9)	33(9)
0.40	30(2)	3.6(5)	5.5(4)	257(5)	28(5)
0.20	28(2)	5.9(5)	8.5(7)	256(4)	29(4)
0.00	25(2)	5.4(5)	9.6(8)	253(3)	32(3)
-0.20	26(2)	5.6(5)	3.4(5)	258(3)	27(3)
-0.40	15(1)	9.9(5)	5.2(4)	260(2)	25(2)
-0.60	14(1)	6.4(5)	6.1(4)	274(2)	11(2)
-0.80	16(1)	5.8(5)	8.6(9)	274(2)	11(2)

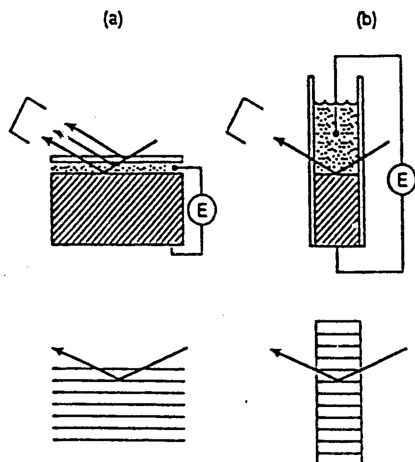

Fig. 1. (a) Reflection (Bragg) geometry. (b) Transmission (Laue) geometry. The upper figures are for the metal/solution interphase and the lower ones are for single crystals.

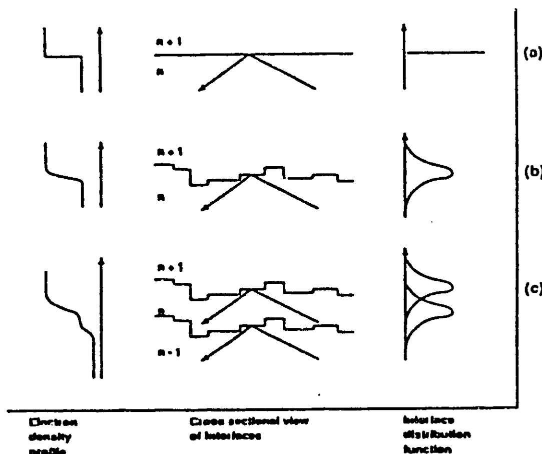

Fig. 3. Three possible interfaces between media: (a) sharp and ideal interface, (b) rough interface, and (c) one sharp and two conformally rough interfaces.

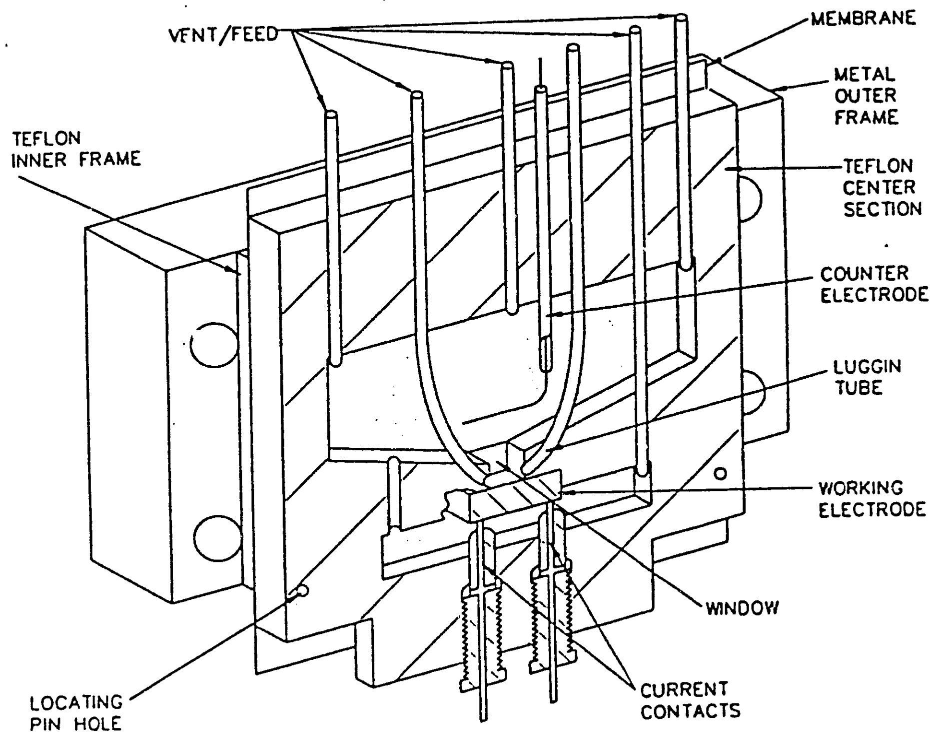

Fig. 2. Transmission-geometry x-ray/electrochemical cell design. Schematic drawings, not to scale.

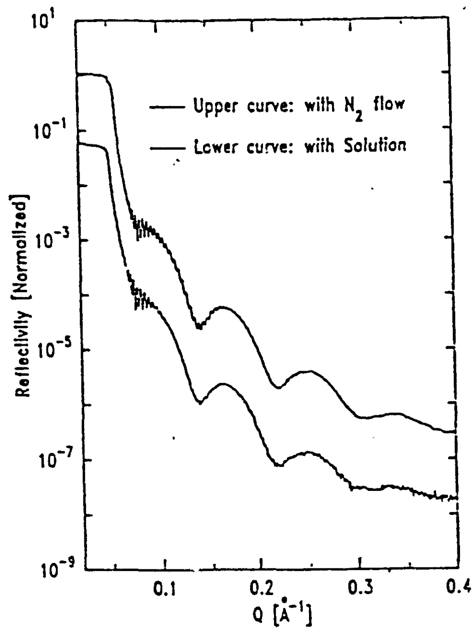

Fig. 4. Spectra of chromium/nickel sandwich indicating the effect of the solution.

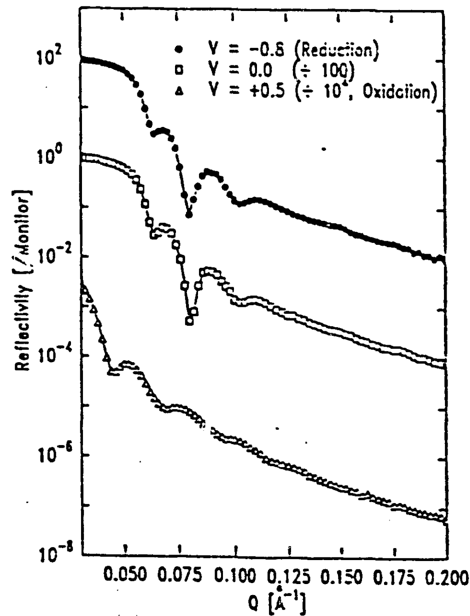

Fig. 5. Spectra of silver film at a series of potentials measured against a Ag/AgCl (3 M KCl) reference electrode.

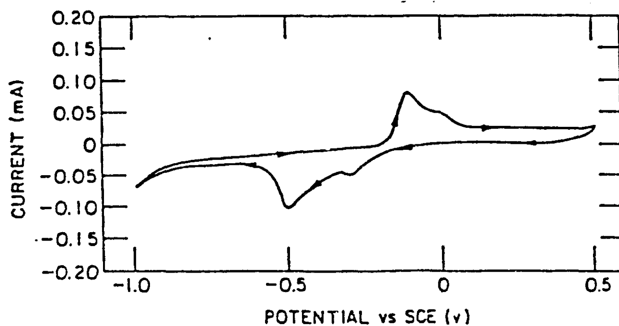

Fig. 6. Cyclic voltammogram of the Cu/Si electrode in borate buffer solution (pH=8.4), scan rate=10 mV/sec.

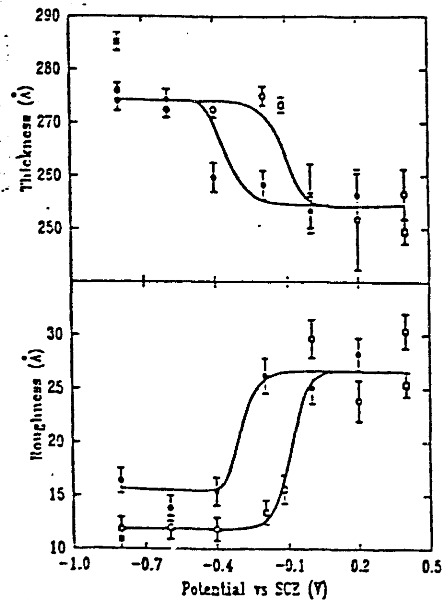

Fig. 8. Selected parameters calculated from scans shown in Fig. 7. (a) The thickness of the copper film on silicon. (b) The conformal roughness of the copper/oxide and oxide/solution interfaces.

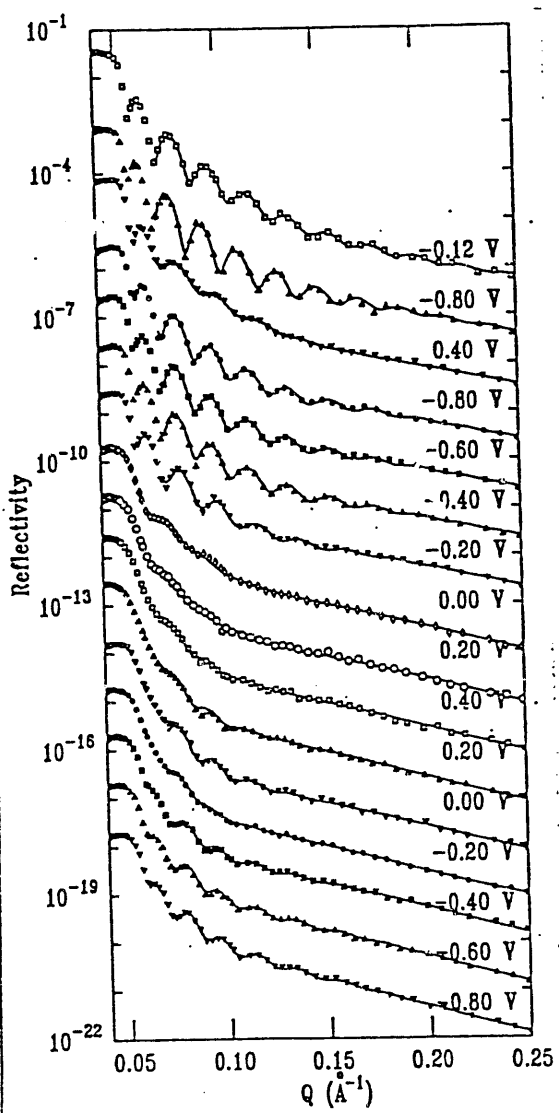

Fig. 7. A series of reflectivity scans for the copper/silicon sample in borate buffer solution made at potentials vs (SCE) indicated. For display purposes, each reflectivity scan was sequentially offset by one order of magnitude.

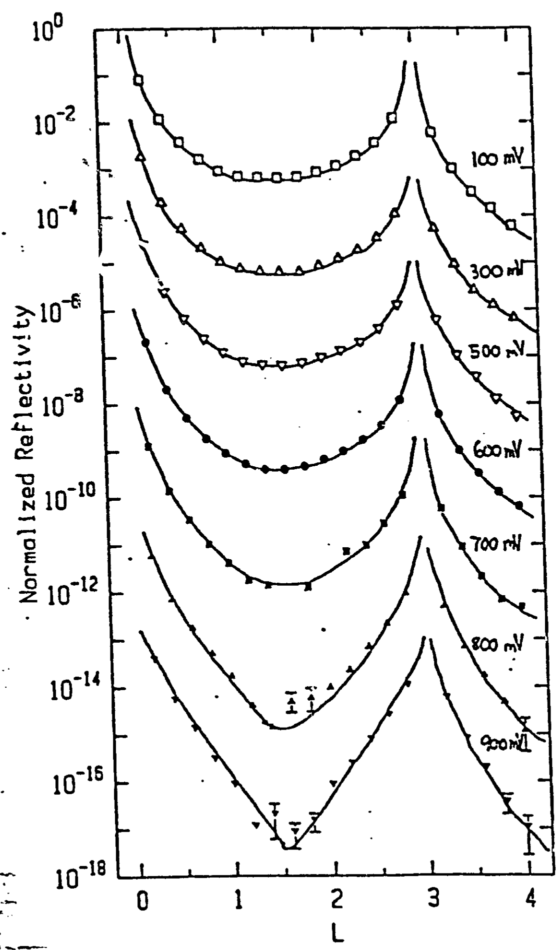

Fig. 9. A series of truncation-rod scans for the platinum(111) crystal in 0.1 M CsF solution with oxidation at potentials (Ag/AgCl, 3 M KCl) indicated. For display purposes, each reflectivity scan was sequentially offset by two orders of magnitude.

END

DATE FILMED

12/17/91